Acta Cryst. (1992). A48, 336-346

Accuracy of Pair Distribution Function Analysis Applied to Crystalline and Non-Crystalline Materials

BY B. H. TOBY* AND T. EGAMI

Department of Materials Science and Engineering and Laboratory for Research on the Structure of Matter, University of Pennsylvania, Philadelphia, Pennsylvania 19104-6272, *USA*

(*Received* 7 *September* 1990; *accepted* 28 *November* 1991)

Abstract

Pair distribution function (PDF) analysis of neutron or X-ray powder diffraction data is a useful technique for analysis of short-range structure in both amorphous and crystalline materials. Errors in PDF determinations may arise from several sources: termination of the Fourier transform, lack of instrument resolution, counting statistics and inaccurate corrections for experimental artifacts. Estimates of the amount of error from termination and instrument resolution are computed using a model structure. A general method for estimating the expected contribution of statistical error to the PDF is introduced for the first time. The effect of termination varies with the type of material and with the amplitude of lattice vibrations but, in general, termination with $Q > 30$ Å produces minimal errors. Broadening of the diffraction pattern produces negligible effect for conventional instrumentation. With moderate data-collection times, the statistical errors can be reduced to reasonable levels. Pulsed-neutron diffraction can provide accurate and precise PDF measurements, as is demonstrated in this work by the agreement between model and experimental results for polycrystalline aluminium.

Introduction

The local atomic structure of materials may be examined without invoking crystallographic symmetry using pair distribution function (PDF) analysis. The PDF, which can be determined by direct Fourier transformation of neutron powder diffraction data, shows the probability of finding any two atoms at a given interatomic distance (Warren, 1969; Klug & Alexander, 1968). A PDF may also be determined with X-rays, as will be discussed later, but the analysis is less straightforward.

The primary application of PDF analysis has been in structural studies of amorphous and liquid materials, which lack lattice periodicity (Cargill, 1975; Wagner, 1972). For these non-crystalline materials, published PDFs generally have broad features with little usable information beyond the second or third coordination sphere and often exhibit large spurious oscillations due to experimental errors. This has led many people to assume incorrectly that PDF analysis provides useful information regarding only very short range interatomic distances and is a method of last resort, to be avoided whenever lattice symmetry can be assumed. In reality, the broad PDF features seen in amorphous materials are due to the wider range of bond distances and angles in these materials. In more ordered solids, the PDF has much more structure and can provide information on the medium-range atomic structure. Furthermore, with modern instrumentation and with careful data reduction, the spurious oscillations can be reduced to minimal levels. As will be presented later, the accuracy and precision to which a PDF may be determined is demonstrated in Fig. 1, where an experimentally determined PDF for polycrystalline aluminium powder at 50 K is compared to the result expected from the crystal structure.

It is well known that one important prerequisite for accurate PDF determination is the measurement of the diffractogram with large momentum transfer, which requires a high-energy (short-wavelength) probe. While this cannot be obtained from standard laboratory diffraction instruments, it is possible to determine accurate and precise pair distribution functions using data from modern high-energy high-intensity synchrotron diffractometers and particularly from neutron spallation sources and time-of-flight detection (for example, see Carpenter & Yelon, 1986). Customized laboratory instrumentation using a tungsten *Bremsstrahlung* source and energy-dispersive detection has also been used with success for PDF analysis (Egami, 1978).

Accurate PDF measurements have been used for crystalline materials to differentiate correlated atomic displacements from random displacements, structural details that are easily missed by standard crystallographic analysis, such as Patterson and direct-methods structure determination and single-crystal and Rietveld refinement techniques (Dmowski *et al.*, 1988; Toby, Egami, Jorgensen & Subramanian, 1990). For crystallographic analysis, the assumption of long-

* Present address: Air Products & Chemicals, Inc., R&D #1, 7201 Hamilton Boulevard, Allentown, Pennsylvania 18195-1501, USA.

0108-7673/92/030336-11$03.00

range translational symmetry superimposes the contents of each unit cell, so that each atomic position in the crystal structure reflects an average. All crystals have deviations from ideal lattice symmetry: atoms have random dynamic displacements due to thermal and zero-point vibration but, in addition, some crystals exhibit correlated dynamic displacements or local static atomic deviations from the ideal symmetry. Unless the correlation length of such displacements is sufficiently large (>100 Å) so that the local structure is reflected in the long-range symmetry of the material, random and correlated atomic displacements may be distinguished only through examination of diffuse scattering. Crystallographic analysis, which uses only Bragg scattering, must treat such displacements as random - using a model with either disordered sites or with anomalously large thermal vibration amplitudes, thus not providing an accurate picture.

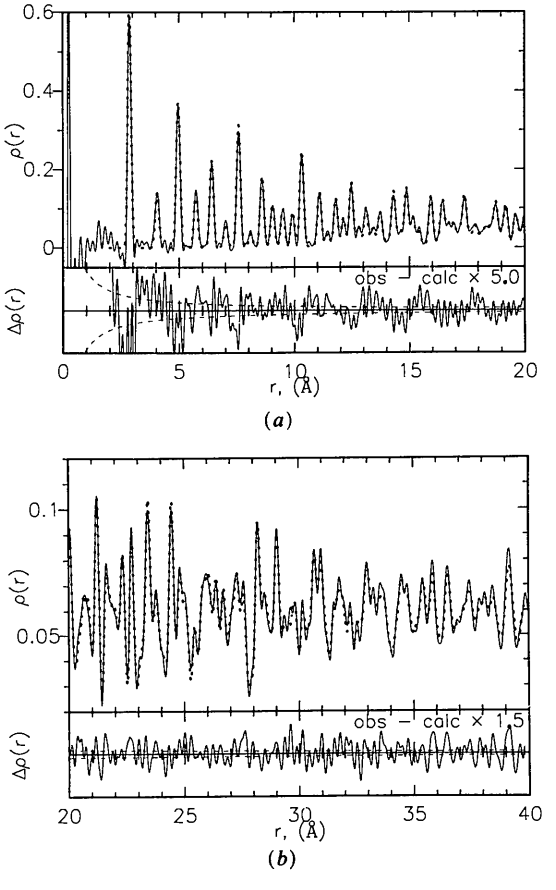

Fig. 1. An observed (solid line) and computed (dotted line) pair distribution function for polycrystalline Al powder at 50 K plotted over the ranges (*a*) 0-20 Å and (*b*) 20-40 Å. The lower box shows the deviation between the observed and calculated results (solid line) and $\pm 1\sigma$ where σ is the standard deviation estimated from counting statistics (dashed line). The lower-box contents are magnified 5:1 for (*a*) and 1.5:1 for (*b*).

In contrast, the PDF is computed using both diffuse and Bragg scattering and does reflect short-range correlations in atomic positions. Thus the PDF can discriminate effectively between short-range order and random displacements, at the cost of giving little information about the long-range structure of a material. Thus the two techniques are highly complementary. Fortunately both can be used for analysis of the same diffraction data.

An example of the utility of PDF measurements is given by the study of the $Tl_2Ba_2CaCu_2O_8$ superconductor, where PDF measurements have demonstrated Tl-O displacements having only short-range order (Dmowski *et al.*, 1988); crystal structure analysis was forced to model the Tl-O plane with a disordered structure (Cox, Torardi, Subramanian, Gopalakrishnan & Sleight, 1988). More careful crystallographic analysis coupled with electron microscopy also confirmed these displacements (Hewat, Hewat, Brynestad, Mook & Specht, 1988). Also, PDF determinations showed unmistakable indications of a change in the short-range structure with the onset of superconductivity, while Rietveld analysis of the same data showed no change in the average structure (Toby *et al.*, 1989, 1990).

This new goal of making qualitative structural measurements from PDF measurements requires a more detailed understanding of the sources of error in PDF measurements. In this paper we discuss both systematic and statistical error sources for PDF measurements and estimate their relative magnitudes.

1. Background

In this section we present the definitions and notation used in PDF analysis, following the descriptions of Lovesey (1984) and Warren (1969). A comparison to crystallographic formulations will also be given. Equations specific to neutron diffraction will be used but, where appropriate, extensions or approximations for X-ray diffraction will be introduced.

1.1. *Diffraction intensity and the structure factor*

The scattering of a probe particle is characterized by the momentum-transfer vector $\mathbf{Q}$, $\mathbf{Q} = \mathbf{k}_f - \mathbf{k}_i$ and energy transfer $\omega = \omega_i - \omega_f$, where $\mathbf{k}_i$ and $\mathbf{k}_f$ are the incident and final momentum vectors and where ω_i and ω_f are the energies of the particle before and after scattering. In the general case, the scattering intensity from a collection of atoms may be written as

$$I(\mathbf{Q}, \omega) = \int_{-\infty}^{\infty} \exp[-i\omega\tau]\langle b\rangle^2 \mathcal{I}(\mathbf{Q}, \tau)\, d\tau \qquad (1)$$

where the total intermediate scattering function, $\mathcal{I}(\mathbf{Q}, \tau)$, describes interference between scattered

waves with time lag τ;

$$\mathcal{I}(\mathbf{Q},\tau)=(\langle b\rangle^2 N)^{-1}\times\left\langle\!\!\left\langle \sum_{j,k} b_j b_k \exp\{i\mathbf{Q}\cdot[\mathbf{r}_j(t)-\mathbf{r}_k(t+\tau)]\}\right\rangle\!\!\right\rangle. \quad (2)$$

In these equations, $\mathbf{r}_j(t)$ is the position of the jth atom at time t, b_j is the scattering length for the jth atom and the summation is performed for all pairs of atoms in the sample. The double angle brackets ($\langle\langle\ldots\rangle\rangle$) indicate a time average and the single brackets ($\langle\ldots\rangle$) indicate a compositional average. Note that the scattering intensity is normalized to unit solid angle of detection and to the number of scatterers and has the same units as b^2 (usually barns, 1 barn $=10^{-28}$ m^2). Equation (1) neglects contributions from multiple scattering and attenuation due to absorption, which depend on the experiment geometry.

Two limiting cases may be considered. In the first case, intensity detection is performed without energy discrimination but with fixed $\mathbf{Q}$, so that all values of ω are sampled. The resulting intensity, $I_{\rm tot}(\mathbf{Q})$, is the integral of $I(\mathbf{Q},\omega)$ for all ω,

$$\begin{aligned} I_{\rm tot}(\mathbf{Q}) &= \int_{-\infty}^{\infty}\int_{-\infty}^{\infty} \exp[-i\omega\tau]\langle b\rangle^2\mathcal{I}(\mathbf{Q},\tau)\,d\tau\,d\omega \\ &= \int_{-\infty}^{\infty} \delta(\tau)\langle b\rangle^2\mathcal{I}(\mathbf{Q},\tau)\,d\tau \\ &= \langle b\rangle^2\mathcal{I}(\mathbf{Q},0) \\ &= N^{-1}\sum_{j,k} b_j b_k\langle\langle\exp\{i\mathbf{Q}\cdot[\mathbf{r}_j(t)-\mathbf{r}_k(t)]\}\rangle\rangle. \end{aligned} \quad (3)$$

Thus, this energy-integrated intensity function is indicative of the instantaneous correlations between atomic positions. It should be noted that for detection at fixed 2θ, $\mathbf{Q}$ will vary with ω since Bragg's law, $Q=|\mathbf{Q}|=4\pi(\sin\theta)/\lambda$, is true only for elastic scattering. Thus, in practice, data collected without energy discrimination will not directly measure $I_{\rm tot}(\mathbf{Q})$ since Q is not constant. The Placzek approximation is customarily applied to correct for the shift in Q with ω (Placzek, 1952).

In the second case, energy discrimination is used to restrict the measurement to elastic scattering ($\omega=0$ and $|\mathbf{k}_i|=|\mathbf{k}_f|$). With the assumption of ideal energy analysis, the elastic scattering intensity, $I_{\rm el}(\mathbf{Q})$, is given by

$$\begin{aligned} I_{\rm el}(\mathbf{Q}) &= \int_{-\infty}^{\infty}\delta(\omega)I(\mathbf{Q},\omega)\,d\omega \\ &= \int_{-\infty}^{\infty}\langle b\rangle^2\mathcal{I}(\mathbf{Q},\tau)\,d\tau \end{aligned} \quad (4)$$

where the delta function represents the energy analysis function. In practice, the measured intensity includes inelastic scattering intensity, with small $|\omega|$, along with the elastic scattering ($\omega=0$), but it is possible to estimate and correct for the contribution of this inelastic intensity. The integration in (4) includes all values of τ, so $I_{\rm el}(\mathbf{Q})$ is independent of any time-dependent correlations in atomic positions and thus the scattering intensity may be considered indicative of what we will refer to as the time-independent structure. Further simplification is possible using $\mathbf{r}_j(t)=\mathbf{u}_j+\mathbf{r}_j(t)$, where $\mathbf{u}_j=\langle\langle\mathbf{r}_j(t)\rangle\rangle$ and by noting the independence of the exponential terms

$$\begin{aligned} I_{\rm el}(\mathbf{Q}) = N^{-1}\sum_{j,k} B_j B_k \exp[i\mathbf{Q}\cdot(\mathbf{r}_j-\mathbf{r}_k)] \\ \times\langle\langle\exp[i\mathbf{Q}\cdot\mathbf{u}_j(t)]\rangle\rangle \\ \times\langle\langle\exp[-i\mathbf{Q}\cdot\mathbf{u}_k(t)]\rangle\rangle. \end{aligned} \quad (5)$$

Thermal and zero-point motion decreases the scattering intensity with increasing Q. The Debye–Waller model assumes vibrational motion to be uncorrelated and approximates the intensity loss as

$$\exp[-Q^2(\langle\langle u_{Q,i}^2\rangle\rangle+\langle\langle u_{Q,k}^2\rangle\rangle)/2],$$

where $u_{Q,j}$ is the component of the vibrational motion of $\mathbf{u}_j$ in the direction $\mathbf{Q}$.

For powder diffraction, a sample composed of a large number of randomly oriented crystallites effectively averages the measurement over all orientations of $\mathbf{Q}$, yielding $I(Q,\omega)$, the powder-averaged scattering intensity. For later use, it will be convenient to define the powder-averaged structure factor, $S(Q)$, which has related definitions for each of the above two cases,

$$S_{\rm tot}(Q)=[I_{\rm tot}(Q)/\langle b\rangle^2]-[(\langle b^2\rangle-\langle b\rangle^2)/\langle b\rangle^2] \quad (6)$$

and

$$\begin{aligned} S_{\rm el}(Q) = [I(Q)/\langle b\rangle^2]-[(\langle b^2\rangle-\langle b\rangle^2)/\langle b\rangle^2] \\ \times\exp(-\langle\langle u_Q^2\rangle\rangle Q^2) \end{aligned} \quad (7)$$

where $\langle\langle u_Q^2\rangle\rangle$ is related to the Debye parameter, B, by $B=8\pi^2\langle\langle u_Q^2\rangle\rangle$. Note that the definition of the structure factor used here differs from the definition for the structure factor, F_{hkl}, used in crystallography, as will be explored further in § 1.4.

For X-rays, scattering factors b_j are no longer constant but vary with Q and are customarily written as $f_j(Q)$, with units of electrons. Except for very unusual experiments, X-ray energy resolution does not allow separation of elastic from phonon-mediated inelastic scattering, so X-ray scattering represents the instantaneous structure, determined by $I_{\rm tot}$.

1.2. *Experimental determination of the structure factor*

Experimentally, it is not possible to measure $I(Q)$ directly and a number of corrections must be applied to the experimental measurements to correct for absorption, polarization, multiple scattering and

either Placzek or inelastic scattering. In addition, corrections are usually required for instrument background and scattering from the sample mounting or container. If an energy-dispersive instrument is used, it is also necessary to normalize to the incident source spectrum.

For our $S(Q)$ determinations from time-of-flight neutron diffraction data, three independent diffractograms are collected for (1) the sample, which includes scattering from the sample container and instrument background; (2) an empty sample container, which also includes the instrument background; (3) the instrument background. In addition, scattering from a vanadium reference standard is used to calibrate the incident-beam monitor and is collected along with each diffractogram to measure the incident spectrum. From these measurements the method of Price (undated) is used to compute $S(Q)$ using

$$S(Q) = C_1(Q)\left[a_1\left(\frac{I_s(Q)}{M_s(Q)} - \frac{I_b(Q)}{M_b(Q)}\right) - a_2\left(\frac{I_c(Q)}{M_c(Q)} - \frac{I_b(Q)}{M_b(Q)}\right)\right] + C_2(Q) \quad (8)$$

where I_s, I_c and I_b are the sample, container and background intensity measurements, respectively, $M(Q)$ indicates the incident spectrum correction computed from the monitor measurement and scaled by the total neutron flux for the measurement, a_1 and a_2 are absorption corrections for the sample and container, respectively, and $C_1(Q)$ and $C_2(Q)$ contain sample- and instrument-dependent scaling factors and corrections for multiple and Placzek scattering (Placzek, 1952). The experimentally obtained $S(Q)$ for polycrystalline aluminium, used to generate Fig. 1, is shown in Fig. 2.

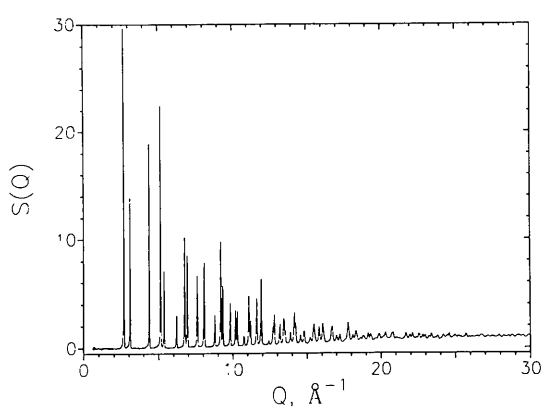

Fig. 2. The observed $S(Q)$ for polycrystalline Al powder at 50 K used to obtain Fig. 1, collected in 2 h using the SEPD time-of-flight diffractometer at the Argonne Intense Pulsed Neutron Source.

1.3. *The pair distribution function*

The pair distribution or pair density function (PDF), $\rho(r)$, for neutron diffraction is defined for the instantaneous structure $\mathbf{r}(t)$ by

$$\rho_{\rm tot}(\mathbf{r}) = N^{-1}\sum_{j\neq k}(b_j b_k/\langle b\rangle^2)\langle\!\langle\delta\{\mathbf{r}-[\mathbf{r}_j(t)-\mathbf{r}_k(t)]\}\rangle\!\rangle. \quad (9)$$

The PDF may be obtained from $S(\mathbf{Q})$ using (3),

$$\rho_{\rm tot}(\mathbf{r}) - \rho_0 = (2\pi)^{-3}\int[S_{\rm tot}(\mathbf{Q})-1]\exp(-i\mathbf{Q}\cdot\mathbf{r})\,d\mathbf{Q} \quad (10)$$

or in the powder-averaged case

$$\rho_{\rm tot}(r) - \rho_0 = (2\pi^2 r)^{-1}\int Q[S_{\rm tot}(Q)-1]\sin Qr\,dQ. \quad (11)$$

Similarly, for the elastic scattering case it is also possible to define a time-independent PDF,

$$\rho_{\rm el}(\mathbf{r}) = N^{-1}\sum_{j\neq k}\langle\!\langle(b_j b_k/\langle b\rangle^2)\delta\{\mathbf{r}-[\mathbf{r}_j(t)-\mathbf{r}_k(t+\tau)]\}\rangle\!\rangle. \quad (12)$$

This PDF can be related to the elastic $S(\mathbf{Q})$ using (4),

$$\rho_{\rm el}(\mathbf{r}) - \rho_0 \simeq (2\pi)^{-3}\int[S_{\rm el}(\mathbf{Q}) - \exp(-\langle\!\langle u_Q^2\rangle\!\rangle Q^2)] \times\exp(-i\mathbf{Q}\cdot\mathbf{r})\,d\mathbf{Q}. \quad (13)$$

However, this equation is approximate due to the assumption of the Debye-Waller model. With the powder-averaged $S_{\rm el}(Q)$,

$$\rho_{\rm el}(\mathbf{r}) - \rho_0 \simeq (2\pi^2 r)^{-1}\int Q[S_{\rm el}(Q) - \exp(-\langle\!\langle u_Q^2\rangle\!\rangle Q^2)] \times(\sin Qr)\,dQ \quad (14)$$

is obtained. Note that at very small r values both PDFs must be zero, since there is a lower limit for interatomic distances due to interatomic repulsions. At large r the PDF approaches the average value ρ_0, because correlation in atomic positions becomes, for both crystalline and amorphous materials, decreasingly discernible for a coordination sphere with increasingly large radius.

The radial distribution function, RDF, is used with different meanings in the literature. While it is sometimes used interchangeably with the PDF, we define the RDF to be $4\pi r^2\rho(r)$ (Cargill, 1975). Note that the number of atoms in a coordination shell with radii $r_{\rm min}$ to $r_{\rm max}$ is defined by

$$\int_{r_{\rm min}}^{r_{\rm max}} 4\pi r^2\rho(r)\,dr.$$

Historically, the PDF has been used to characterize only near-neighbor distances but, for many materials, the PDF shows sufficient detail that it may be used for more general structural determination. While the PDF is likely to exhibit some overlap of peaks, comparison may still be made to a model PDF in a manner analogous to Rietveld analysis, provided the comparison is made over a wide range in r. We define an

agreement factor, A, to measure the discrepancies between an experimental and a model PDF over a range in r, r_{min} to r_{max}, as

$$A^2 = \rho_0^{-2}(r_{max} - r_{min})^{-1} \int_{r_{min}}^{r_{max}} [\rho_{obs}(r) - \rho_{model}(r)]^2 \, dr. \quad (15)$$

For the case where both functions have been evaluated at n points spaced equally in r, the PDF agreement factor can be written as

$$A^2 = (n\rho_0^2)^{-1} \sum_{i=1}^{n} [\rho_{obs}(r_i) - \rho_{model}(r_i)]^2. \quad (16)$$

For X-ray diffraction, a PDF may be defined analogously to (9) using the Warren–Krutter–Morningstar approximation (Warren, Krutter & Morningstar, 1936), where the atomic scattering factor $f_j(Q)$ is approximated as $b_j f_{avg}(Q)$, where b_j is a constant approximately equal to the number of electrons in element j and $f_{avg}(Q)$ is the average normalized Q dependence for all elements in the material. The Fourier transform relation of (11) then becomes approximate. However, since the scaled Q dependence of $f_j(Q)$ for different elements are comparable, the approximation is reasonably good.

1.4. *Comparison to crystallographic notation*

The momentum transfer vector, $\mathbf{Q}$, is usually expressed in crystallographic terms using general indices hkl to indicate a Bragg reflection, where $\mathbf{Q} = 2\pi(h\mathbf{a}^* + k\mathbf{b}^* + l\mathbf{c}^*)$. For an ideal crystal, $S(Q)$ can be expressed in terms of the crystallographic structure factor, F_{hkl}, with hkl equivalent to $\mathbf{Q}$,

$$\int_{\delta V_Q} S(\mathbf{Q}) \, d\mathbf{Q} = \frac{8\pi^3}{v_c} \frac{1}{n_c} \frac{1}{\langle b^2 \rangle} F_{hkl}^2 \quad (17)$$

where v_c is the unit-cell volume, n_c is the number of atoms in the unit cell, δV_Q is a small volume in reciprocal space surrounding reflection hkl. The customary definition of the crystallographic structure factor, F_{hkl}, is

$$F_{hkl} = \sum_{j=1}^{n_c} \rho(x, y, z) \exp[2\pi i(hx_j + ky_j + lz_j)] \quad (18)$$

where $\rho(x, y, z)$ represents the probability of finding a unit scatterer at position (x, y, z). In the Debye–Waller model, it is assumed that each atom vibrates around a fixed position, (x_j, y_j, z_j), with amplitude proportional to B_j (isotropic vibration) or with a component $B_{Q,j}$ in the direction of $\mathbf{Q}$ (anisotropic vibration), where $B_{Q,j}$ is related to the mean-square displacement in direction $\mathbf{Q}$ by $B_{Q,j} = 8\pi^2 \langle\langle u_{Q,j}^2 \rangle\rangle$. The crystallographic structure factor may then be written

$$F_{hkl} = \sum_{j=1}^{n_c} b_j \exp(-B_j Q^2/16\pi^2) \times \exp[-2\pi i(hx_j + ky_j + lz_j)]. \quad (19)$$

For X-rays, again the substitution $f_j(Q)$ is made for b_j and the unit scatterer is an electron.

Note that the total structure factor, $S(Q)$, is defined per unit volume in reciprocal space, while the crystallographic structure factor F_{hkl} is the integral of the Bragg peak at hkl. Thus, when determining the crystallographic structure factor, it is necessary to apply a Lorentz correction (also referred to as the geometrical part of the Lorentz–polarization correction) to the observed intensities to correct for the volume of reciprocal space sampled in the measurement. However, this correction is not needed for determination of the PDF.

For the powder-averaged structure factor, reflections will overlap, since Q can be equal or nearly equal for different values of hkl, so

$$S(Q) = (2\pi^2/V_c)(n_c\langle b^2 \rangle Q^2 \delta Q)^{-1} \sum_{Q}^{Q+\delta Q} F_{hkl}^2 \quad (20)$$

where the sum is over all reflections with momentum transfer between Q and $Q + \delta Q$. The factor $Q^2\delta Q$ in this equation is the aforementioned Lorentz factor evaluated in Q.

For crystallographic error analysis, discrepancies between observed and calculated F values are reported using different formulations of weighted or unweighted residuals, commonly referred to as the R factor. These expressions are analogous to the formulation used for the PDF agreement factor [(8)]. However, it should be noted that the crystallographic R factor gives greatest weight to the data at low Q, where diffraction intensities are largest. This is in contrast to the PDF agreement factor, which gives most weight to the high-Q data that are most significant for PDF computation. Thus, the crystallographic R factor stresses agreement in long-range order, while the PDF agreement factor stresses agreement in short-range order.

1.5. *Modeling of pair distribution functions*

The PDF for a collection of atoms may be computed by counting the interatomic distances between every possible pair of atoms, weighted by b_j for each atom. To incorporate the broadening effects of thermal motion, two different approaches are commonly used: either a model with a large number of atoms is used and each atom is given random displacements, or the PDF from a smaller model is computed and is then convoluted with a Gaussian broadening function,

$$\sigma(2\pi)^{-1/2} \exp(-\Delta r^2/2\sigma^2) \quad (21)$$

where

$$\sigma = (\langle\langle u_{r,j}^2\rangle\rangle + \langle\langle u_{r,k}^2\rangle\rangle)^{1/2} = (B_{r,j} + B_{r,k})^{1/2}/(8^{1/2}\pi)$$

and $\langle\langle u_{r,j}^2\rangle\rangle$ and $B_{r,j}$ are defined as before but are the components in the direction $\mathbf{r}_j - \mathbf{r}_k$. This latter method has been used with success for PDF modeling of crystalline materials [see Egami (1990) for examples] and offers the advantage of computational simplicity and ease of analysis because local distortions are not masked by random 'thermal' displacements.

The simulated PDF shown in Fig. 1 was computed by counting distances between a single Al atom and all other atoms in an infinite face-centered cubic (f.c.c.) lattice. The PDF was then broadened by convolution with a Gaussian. For the instantaneous PDF, bonding interactions will introduce correlation in vibration between nearest-neighbor atoms, which will lead to decreased broadening of the PDF peaks at small r. Thus it is necessary to broaden the first peak with a slightly narrower Gaussian. For the simulated PDF in Fig. 1, the first peak was broadened by a Gaussian with $\sigma = 0.073$ Å while, for peaks at larger r, $\sigma \simeq 0.082$ Å was used.

2. Sources of error in PDF determination

Experimental errors in PDF determinations may arise from a number of sources. Three such sources, termination, instrument resolution and counting statistics are readily identifiable and will be discussed explicitly in the following paragraphs. Another possible source of errors is inaccuracies in the experimental corrections that are applied to diffraction intensities to obtain $S(Q)$; the expected result of such errors is also discussed below.

To measure the effects of these experimental factors on PDF determination, ideal total structure factors, $S(Q)$, were computed for crystalline aluminium by mapping the computed crystallographic structure factors onto a grid with a fixed Q spacing. Since the point spacing introduces small errors into the PDF, the number of points in the grid was increased (to 500 points per Å^{-1}) so that the differences in the PDF were very small.

2.1. *Termination errors*

For an infinitely precise computation of a PDF, $\rho(r)$, it is necessary to perform the Fourier-sine transformation of $Q[S(Q)-1]$ in (11) or (14) over all values of Q from zero to infinity. However, the Q values that can be accessed experimentally are limited by instrument design to a range $Q_{\min} \le Q \le Q_{\max}$. The quality of collimation usually dictates $Q_{\min}$; for most instruments $Q_{\min}$ is sufficiently small that the terms missing from the transform are of negligible importance, since they are multiplied by Q. The energy or wavelength of the neutron or X-ray probe limits $Q_{\max}$, since $Q_{\max} = 4\pi(\sin\theta)/\lambda < 4\pi/\lambda$ where $\lambda = hc/E$ for X-rays and $\lambda^2 = h^2/(2M_nE)$ for neutrons. The omission of terms with $Q > Q_{\max}$ frequently results in spurious oscillations [see Cargill (1975) and Suzuki (1986) for discussion]. The termination of the PDF computation at $Q_{\max}$ is equivalent to multiplication of $S(Q)$ by a step function, so this causes $\rho(r) - \rho_0$ to be convoluted with a broadening function, $\sin(Q_{\max}\Delta r)/\Delta r$, the Fourier transform of the step function. However, since thermal and zero-point motion always broadens the PDF, it is possible to choose a minimum value for $Q_{\max}$ such that the additional broadening due to termination is negligible with respect to the thermal broadening.

To serve as a quantitative reference for determination of the $Q_{\max}$ value needed to guarantee that termination effects are small with respect to thermal motion, a model computation was performed where a Debye–Waller damping function was applied to the ideal structure factor for a f.c.c. structure. The PDF was obtained by Fourier transform of the damped $S(Q)$ with truncation at selected values of Q. The agreement factor between the PDF simulated from the ideal crystal structure and convoluted with a Gaussian of appropriate width and the PDF with truncation was computed using (16). Displayed in Fig. 3 are the results for values of the Debye–Waller temperature factor, B, of 0.28, 0.39 and 0.92 Å^2, corresponding to the estimated vibration amplitudes for crystalline aluminium at 0, 100 and 295 K (*International Tables for X-ray Crystallography*, 1968). These temperature factors lead to broadening of the PDF with $\sigma = 0.084$, 0.100 and 0.153 Å, respectively. Also displayed are results using B values for the estimated zero-point vibration for Ni, 0.1 Å^2, and Cu, 0.14 Å^2, which correspond to σ values of 0.05 and 0.06 Å,

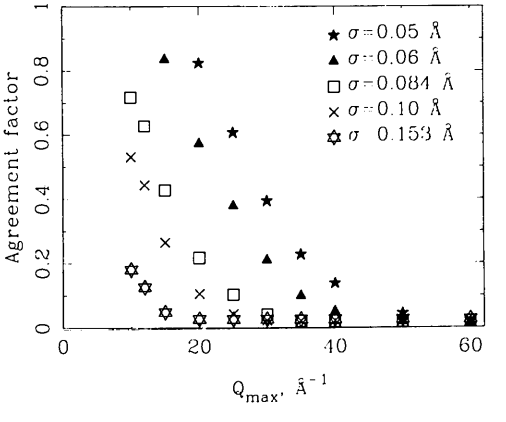

Fig. 3. The amount of error introduced into the PDF due to termination of $S(Q)$ at different values of $Q_{\max}$ with values of the Debye–Waller temperature factor, B, of 0.1, 0.14, 0.28, 0.39 and 0.92 Å^2 (filled stars, filled triangles, squares, crosses and six-pointed stars, respectively). Agreement is computed over the range $r = 2$ to 20 Å by comparison to an ideal PDF with appropriate broadening (computed as described in the text).

respectively (*International Tables for X-ray Crystallography*, 1968). Except at very low temperatures, most materials exhibit thermal vibration greater than that for Al at 0 K, so termination at 30 $Å^{-1}$ will be sufficient for accurate determination of the PDF. Amorphous materials and quasicrystals tend to have much broader features in their PDFs than crystalline materials so truncation errors are less severe.

When high-Q data cannot be collected, many workers apply a damping function to reduce the intensities of the high-Q data. The effect of such treatment improves the PDF by reducing spurious oscillations, but it is well known that the resulting PDF has broadened features, since damping is analogous to raising the sample temperature (Bragg & West, 1930). In previous RDF measurements of crystalline aluminium by Ruppersberg & Seemann (1965) and Fessler, Kaplow & Averbach (1966), elevated sample temperatures were used to reduce the errors introduced by termination. Neither damping nor use of elevated temperatures can substitute for measurement of the actual data at high Q, since the degraded resolution due to additional or simulated thermal motion will often obscure significant structural details. Methods for reducing the errors due to termination have been proposed. For example, Kaplow, Strong & Averbach (1965) use an iterative procedure to extrapolate high-Q data by setting $\rho(r)$ to zero for $r \ll r_{\min}$, where $r_{\min}$ is the minimum nearest-neighbor distance. However, Aur (1981) found that, while this procedure did remove spurious oscillations below $r_{\min}$, it did not significantly remove the spurious oscillations introduced by termination above $r_{\min}$. There is no substitute for direct measurement of $S(Q)$ to sufficiently large Q.

2.2. *Instrument resolution*

The inability of diffraction instruments to resolve all of the detail in $I(Q)$ leads to a broadening of diffraction maxima which can be modeled by convolution by an instrument response function. While the instrument response function may have complex dependence on Q, it is often modeled using a Gaussian convolution function,

$$[(2\pi)^{1/2}\sigma_Q^2]^{-1} \exp[-(Q-Q_0)^2/2\sigma_Q^2],$$

where the response function has constant full width at half-maximum $\sigma_Q(8 \ln 2)^{1/2}$. The result from this model is the multiplication of $\rho(r)-\rho_0$ by a broad envelope function,

$$\rho_{\text{apparent}} - \rho_0 = [\rho_{\text{actual}} - \rho_0] \exp(-\tfrac{1}{2}r^2\sigma_Q^2), \quad (22)$$

the Fourier transform of the Gaussian instrument response function. A plot of the degradation of the agreement factor as a function of increasing instrument broadening is shown in Fig. 4.

For some instruments, a more appropriate model for the instrument response function has a loss of resolution proportional to the modulus of the scattering vector, Q, rather than constant for all Q. In Fig. 5, a plot is shown of the error introduced into the PDF where a Q-dependent instrument response function, broadening with $\sigma_Q \propto Q$ ($\Delta Q/Q$ constant), is applied to $S(Q)$. Application of a best-fit Gaussian envelope correction function gave little improvement in discrepancies introduced by the convolution, but allowing the PDF peak width to vary with r, $\sigma_r =$

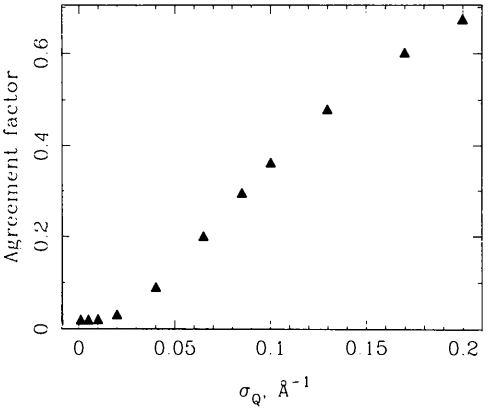

Fig. 4. The change in agreement factor due to a constant-width instrument response function obtained by comparison of the PDF computed from an ideal $S(Q)$ for polycrystalline Al convoluted by a Gaussian function of constant width, σ_Q, with the PDF computed directly from the model structure. Agreement factors are evaluated as defined in the text over the range of 2 to 20 Å. The small deviations of the agreement factor from zero for small values of σ_Q is due to computational limitations.

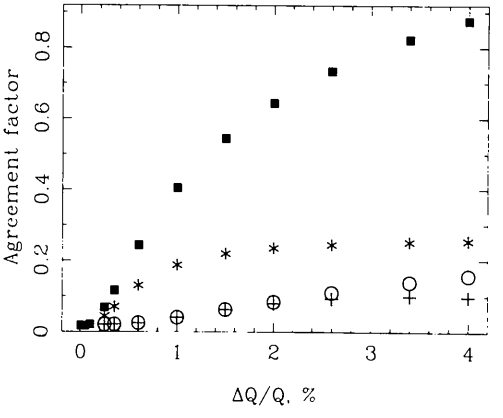

Fig. 5. The change in agreement factor due to a Q-dependent instrument response function obtained by comparison of the PDF computed from an ideal $S(Q)$ for polycrystalline Al convoluted with a Gaussian function of width proportional to Q (squares) and a PDF computed directly from the model structure. Agreement factors are evaluated as defined in the text over the range of 2 to 20 Å. Also shown is the agreement after correction of the model PDF with an r-dependent broadening term (asterisks); multiplication by a Gaussian envelope function (circles); both corrections together (crosses).

$\sigma_0+\alpha r^2$, did give considerably better agreement. Use of both the peak width and the envelope corrections together gave the best agreement, but this becomes noticeable only when the model instrument response function is quite poor or r is greater than 20 Å.

In general, at very large r values, $\rho(r)$ is largely featureless, so loss of resolution and intensity in the PDF at large r provides little impediment to the use of instruments with poor resolution for PDF structural analysis. This is in contrast to crystallographic methods which are often resolution-limited. While it is never possible to recover the information lost due to instrumental broadening, good agreement between the observed and model PDFs over a large range in r may still be obtained by incorporation of appropriate correction terms into the model PDF computation. Thus, regions of the PDF that are significantly affected by instrument broadening may be used for modeling.

For the SEPD instrument at Argonne National Laboratory, instrument resolutions of better than 0.4% $\Delta Q/Q$ are routinely obtained. Experimentally, lack of resolution on this level results in a small increase in the widths of PDF peaks with increasing r, and a minor damping of the PDF at larger r values. The corrections become significant for r greater than 10 Å and either term may be applied alone for satisfactory correction of the PDF for r below 20 Å. The primary effects of the PDF broadening due to the instrumental broadening of $I(Q)$ can be well corrected, as is demonstrated by the goodness of agreement between the observed and model PDF in Fig. 1. The model PDF was computed using a Gaussian convolution where σ is 0.0733 for the first peak and $0.0819+0.000024r^2$ for the remainder of the PDF. In addition, an envelope correction function, $\exp[-(0.0262r)^2/2]$ was applied to the calculated $\rho(r)-\rho_0$.

2.3. *Counting statistics*

Counts of discrete events are subject to statistical fluctuations that are governed by the number of events recorded. The expected or estimated standard deviation (e.s.d.) for the observation N counts is $(N)^{1/2}$. This error is directly germane to most types of diffraction measurements, since counting of individual quanta (neutrons, electrons or photons) is the most precise method for measurement of diffraction intensities.

The estimated errors for a set of observations may be propagated to estimate the error in a function determined from these observables. In general form, the e.s.d. for a function f evaluated using a set of independent observations, $O_1, O_2, \ldots, O_N$, can be estimated from the e.s.d. of each of the observations using

$$\sigma_f^2=\sum_j^N\left[\sigma_{O_j}\frac{\partial f}{\partial O_j}\right]^2 \tag{23}$$

(Hamilton, 1964). If $S(Q)$ is treated as a continuous function, the e.s.d. for $\rho(r)$ can be estimated using

$$\sigma^2_{\rho(r)}=\sum_j^N\sigma^2_{O_j}\left(\frac{\partial\rho(r)}{\partial S(Q)}\right)^2\left(\frac{\partial S(Q)}{\partial O_j}\right)^2. \tag{24}$$

Alternatively, the discrete $S(Q_k)$ points may be treated as independent observables provided that each intensity observation is used to determine only one $S(Q_k)$ value. In this case the e.s.d. for $S(Q_k)$ is given by

$$\sigma^2_{S(Q_k)}=\sum_j^M\sigma^2_{O_j}\left(\frac{\partial S(Q_k)}{\partial O_j}\right)^2 \tag{25}$$

where there are M independent observations of the sample, sample container and background intensities that are used to determine $S(Q_k)$. The computation of the e.s.d. for $\rho(r)$ may then be simplified to

$$\sigma^2_{\rho(r)}=(2\pi^2r)^{-2}\sum_k[\sigma_{S(Q_k)}Q_k\Delta Q_k\sin Q_kr]^2. \tag{26}$$

Equations (25) and (26) may be evaluated directly for estimation of statistical errors. For example, in our neutron time-of-flight analysis we use

$$\sigma^2_{S(Q_j)}=[C_1(Q_j)]^2\left\{\left[\frac{a_1}{M_s(Q)}\sigma_{I_s}\right]^2+\left[\frac{a_2}{M_c(Q)}\sigma_{I_c}\right]^2+\left[\frac{a_1-a_2}{M_b(Q)}\sigma_{I_b}\right]^2\right\}, \tag{27}$$

where the contributions to the statistical error from the incident-spectrum corrections, $M(Q)$, are assumed to be negligible. The estimated error due to counting statistics for the observed aluminium PDF is shown in the lower box of Fig. 1. It is noteworthy that these low error levels are obtained after only 2 h of data collection for a relatively weakly scattering material.

Note that application of a smoothing correction to $S(Q)$ would introduce correlation between the data points, invalidating the simplifications used above. Moreover, smoothing by averaging or filtering can remove oscillations from $S(Q)$ that are believed to be spurious, but such 'improvements' are at best cosmetic and do not reduce errors in the PDF. Use of a Fourier filter to remove high-frequency components will have little effect on the PDF except at very large r, where the PDF is essentially flat. Moving-spline smoothing functions and related methods compute a moving average of the data points, which yields approximately the same results as would be obtained by reducing the number of $S(Q)$ data points by direct averaging. Since smoothing introduces no new observations, it cannot reduce the estimated errors.

2.4. *Optimum data-collection strategy*

In laboratory practice, a limited amount of time may be devoted to measurement of diffraction

intensities for a given sample and the optimum data-collection method will apportion the time for each measurement so that the most precise PDF will be obtained for the total time available. We define a scan-rate function, $R(Q_k)$, using

$$N_{obs}(Q_k) = R(Q_k)\Delta Q_k I(Q_k) = R(Q_k)\Delta Q_k \langle b\rangle^2 S(Q_k), \quad (28)$$

where $N_{obs}(Q_k)$ is the total number of counts for the kth point, $R(Q_k)\Delta Q_k$ is proportional to the counting time or spectral brightness. If we ignore the contributions to the statistical error from experimental corrections including background subtraction, from (25), the e.s.d. for $S(Q)$ is

$$\sigma^2_{S(Q_k)} = S(Q)[R(Q_k)\Delta Q_k \langle b\rangle^2]^{-1}. \quad (29)$$

Use of (26) yields

$$\sigma^2_{\rho(r)} = (2\pi^2 r)^{-2} \sum_k [S(Q_k)/R(Q)\langle b\rangle^2] Q_k^2 \times \sin^2 Q_k r \Delta Q_k, \quad (30)$$

or, equivalently, with $S(Q)$ and $R(Q)$ expressed as continuous functions,

$$\sigma^2_{\rho(r)} = (2\pi^2 r)^{-2} \int [Q^2/R(Q)\langle b\rangle^2] S(Q) \times (\sin^2 Qr)\, dQ. \quad (31)$$

Note that $\langle\langle \sin^2 Qr\rangle\rangle_Q \simeq \frac{1}{2}$, where $\langle\langle \ldots \rangle\rangle_Q$ indicates an average over a wide range in Q, so it is possible to approximate (31) as

$$\sigma^2_{\rho(r)} \simeq (8\pi^4 r^2)^{-1} \int \frac{S(Q)Q^2}{R(Q)\langle b\rangle^2}\, dQ. \quad (32)$$

Thus, it can be seen that the e.s.d. for $\rho(r)$ falls as $1/r$.

Equation (32) can then be used to determine the optimum scan rate, $R(Q)$, which yields the smallest e.s.d.s for $\rho(r)$ for a given total data-collection period. Imposition of a normalization condition for the total scan time, $\int R(Q)\, dQ$ constant, yields

$$\sigma^2_{\rho(r)} \simeq (8\pi^4 r^2)^{-1} \int R(Q)\, dQ \times \int [S(Q)Q^2/R(Q)\langle b\rangle^2]\, dQ. \quad (33)$$

For example, if $R(Q)$ is invariant with Q, the e.s.d. for $\rho(r)$ is

$$\sigma^2_{\rho(r)} \simeq (8\pi^4 r^2)^{-1} \int dQ \int [S(Q)Q^2/\langle b\rangle^2]\, dQ. \quad (34)$$

The optimum e.s.d. will be obtained when

$$R(Q) \propto Q[S(Q)]^{1/2}/\langle b\rangle = Q[I(Q)]^{1/2}/\langle b\rangle^2, \quad (35)$$

because

$$\sigma^2_{\rho(r)} \simeq (8\pi^4 r^2)^{-1} (\int \{Q[S(Q)]^{1/2}/\langle b\rangle\}\, dQ)^2. \quad (36)$$

In contrast, the practice of making intensity measurements to a constant I_{obs} value, so that all measurements are made to the same relative precision, will result in larger than optimal e.s.d.s. In this case, $R(Q) \propto 1/I(Q)$ and

$$\sigma^2_{\rho(r)} \simeq (8\pi^4 r^2)^{-1} \int dQ/[S(Q)\langle b\rangle^2] \int [QS(Q)]^2\, dQ, \quad (37)$$

which yields larger e.s.d.s than (36).

During data collection, the e.s.d. for the PDF may be estimated quickly from the following procedure. With the approximation $\langle\langle S(Q)\rangle\rangle_Q \simeq 1$ and a computation of the total number of counts collected in each region of Q, $N_{tot}(Q_i)$, the e.s.d. may then be estimated using

$$\sigma^2_{\rho(r)} \simeq (8\pi^4 r^2)^{-1} \sum [Q_i^2/N_{tot}(Q_i)][\Delta Q_i]^2. \quad (38)$$

The averaging should be performed in sufficiently large regions, for example of 1 Å^{-1}, so that the structure in $S(Q)$ is averaged out.

2.5. *Experimental corrections*

As previously discussed, corrections for absorption, multiple scattering, inelastic or Placzek scattering, sample container and background scattering must be added to or subtracted from the observed intensity measurements to determine $S(Q)$. Any inaccuracies in these corrections will introduce systematic errors to the computation of $\rho(r)$. However, these experimental effects are broad smoothly varying functions of Q. Thus any systematic errors due to these corrections (the deviations between the applied corrections and the true effects) can also be expected to be broad smoothly varying functions of Q. Adding such a slowly varying error function to $S(Q)$ will add to $\rho(r)$ an error function that decreases in magnitude as r increases. These spurious oscillations in $\rho(r)$ are often readily identifiable because they have a frequency in r typically much greater than structural details.

The observed and computed PDFs for aluminium shown in Fig. 1, while in very good agreement, still have significantly larger deviations than would be expected from counting statistics and termination errors alone. The agreement factors computed using (16) for these PDFs are 0.156 and 0.045 over the ranges 2–20 and 20–40 Å, respectively. In contrast, the statistically expected agreement factors for the same ranges are 0.052 and 0.012, respectively. The discrepancies between the observed and expected agreement factors indicate systematic errors introduced by inaccuracies in the data-analysis procedures and uncorrected systematic errors in the experimental measurements. A PDF determination of a standard material such as this provides a direct measurement of the level of systematic error in the determination.

3. Discussion

Several points concerning PDF analysis have been demonstrated by these investigations. Most significantly, it is possible to make both accurate and

precise determinations of the PDF with modern neutron and synchrotron instrumentation, provided a diffraction probe with sufficiently high energy is used so that termination errors are minimized. In most cases, instrumental broadening does not result in a significant loss of information in the PDF. When poor resolution does produce a noticeable degradation of the PDF, good agreement with a model PDF may still be obtained by incorporation of correction terms into the model PDF computation.

Statistical error can be significant in PDF analysis, as is the case for all diffraction measurements. It has been demonstrated here how one may estimate the magnitude of statistical error in the PDF. As is the accepted practice for crystallographic measurements, all PDF determinations should include a calculation of the estimated statistical error, which may be obtained from propagation of the estimated errors for the intensity measurements to $S(Q)$ and application of (26).

Systematic errors introduced in the collection and processing of diffraction data can limit the quality of the results. As discussed previously, corrections must be applied for instrument calibration, multiple scattering, inelastic scattering, absorption and background. Standard practice for PDF determination should also include periodic determination of a PDF for a material with a well known structure to quantify the level of systematic errors.

As mentioned previously, the deviations between the observed and computed PDFs of aluminium shown in Fig. 1 are larger than that which can be attributed to statistical and termination errors. These systematic errors are attributed to inadequacies in the data processing. The approximations used in such processing, for calculation of experimental corrections such as the Placzek and multiple-scattering corrections, should be re-examined now that termination and statistical errors need not limit the accuracy of PDF analysis and since larger-scale computations are more accessible. Reduction or better characterization of background and container scattering may also significantly improve PDF computations.

Significantly, for certain experiments, the contribution of systematic errors to the PDF can be minimized. For example, when comparing PDFs for a single sample obtained from diffraction measurements under nearly identical conditions, while a single experimental parameter (for example temperature) is changed, the most important error source for differences between the observed PDFs will be statistical in nature. This is likewise true for the case of isomorphic substitution.

In conclusion, PDF analysis can be improved by development of diffraction instruments with lower levels of background and better statistics at high Q, even at the expense of decreased resolution. Improved data-collection strategies can further minimize statistical error in the PDF. It is already possible to obtain accurate PDFs, nearly free from termination errors, as demonstrated by the good agreement shown with a standard material, where the discrepancies are reduced to the same order of magnitude as the statistical error.

The technique has already demonstrated a unique value for analysis of local order in crystalline materials, in addition to the traditional applications to amorphous materials. Improvements to data-processing techniques are needed to take best advantage of the high-quality diffraction data that can be measured with spallation and synchrotron sources.

The authors are grateful to H. D. Rosenfeld for useful discussions. Work at the University of Pennsylvania was supported by the National Science Foundation through grants DMR90-01704 and DMR88-19885. The Intense Pulsed Neutron Source is operated as a user facility by the US Department of Energy, Division of Materials Sciences, under contract W-31-109-Eng-38.

References

AUR, S.-W. (1981). PhD thesis, Univ. of Pennsylvania, USA.
BRAGG, W. L. & WEST, J. (1930). *Philos. Mag.* **10**, 823-841.
CARGILL, G. S. III (1975). *Solid State Phys.* **30**, 227-320.
CARPENTER, J. M. & YELON, W. B. (1986). In *Neutron Scattering*, edited by K. SKÖLD & D. L. PRICE, Part A, pp. 99-196. New York: Academic Press.
COX, D. E., TORARDI, C. C., SUBRAMANIAN, M. A., GOPALAKRISHNAN, J. & SLEIGHT, A. W. (1988). *Phys. Rev. B*, **38**, 6624-6630.
DMOWSKI, W., TOBY, B. H., EGAMI, T., SUBRAMANIAN, M. A., GOPALAKRISHNAN, J. & SLEIGHT, A. W. (1988). *Phys. Rev. Lett.* **61**, 2608-2611.
EGAMI, T. (1978). *J. Mater. Sci.* **13**, 2587-2599.
EGAMI, T. (1990). *Mater. Trans.* **31**, 163-176.
FESSLER, R. R., KAPLOW, R. & AVERBACH, B. L. (1966). *Phys. Rev.* **150**, 34-43.
HAMILTON, W. C. (1964). *Statistics in Physical Science*, pp. 32-34. New York: Ronald Press.
HEWAT, A. W., HEWAT, E. A., BRYNESTAD, J., MOOK, H. A. & SPECHT, E. D. (1988). *Physica (Utrecht)*, C**152**, 438-444.
International Tables for X-ray Crystallography (1968). Vol. III. Birmingham: Kynoch Press. (Present distributor Kluwer Academic Publishers, Dordrecht.)
KAPLOW, R., STRONG, S. L. & AVERBACH, B. L. (1965). *Phys. Rev. A*, **138**, 1336-1345.
KLUG, H. P. & ALEXANDER, L. E. (1968). *X-ray Diffraction Procedures for Polycrystalline and Amorphous Materials*, 2nd ed. New York: Wiley.
LOVESEY, S. W. (1984). *Theory of Neutron Scattering from Condensed Matter*, Vol. 1. Oxford: Clarendon Press.
PLACZEK, G. (1952). *Phys. Rev.* **86**, 377-388.
PRICE, D. L. (undated). *Analysis of Time-of-Flight Neutron Diffraction Data from Isotropic Samples.* IPNS Note 19. Argonne National Laboratory, Illinois, USA.
RUPPERSBERG, H. & SEEMANN, H. J. (1965). *Z. Naturforsch. Tell A*, **20**, 104-109.
SUZUKI, K. (1986). In *Neutron Scattering*, edited by K. SKÖLD & D. L. PRICE, Part B, pp. 243-302. New York: Academic Press.
TOBY, B. H., DMOWSKI, W., EGAMI, T., JORGENSEN, J. D., SUBRAMANIAN, M. A., GOPALAKRISHNAN, J., SLEIGHT, A. W. & PARISE, J. B. (1989). *Physica (Utrecht)*, C**162-164**, 101-102.

TOBY, B. H., EGAMI, T., JORGENSEN, J. D. & SUBRAMANIAN, M. A. (1990). *Phys. Rev. Lett.* **64**, 2414-2417.
WAGNER, C. N. J. (1972). In *Liquid Metals, Chemistry and Physics*, edited by S. Z. BEER, pp. 257-329. New York: Marcel Dekker.
WARREN, B. E. (1969). *X-ray Diffraction*. Reading: Addison-Wesley; New York: Dover.
WARREN, B. E., KRUTTER, H. & MORNINGSTAR, O. (1936). *J. Am. Ceram. Soc.* **19**, 202-206.

Acta Cryst. (1992). A**48**, 346-349

Fast Fourier Transforms for Space Groups Containing Rotation Axes of Order Three and Higher

BY M. AN
Center for Large Scale Computation, City University of New York, New York, NY 10036-8099, *USA*

C. LU
Department of Computer and Information Sciences, Towson State University, Towson, MD 21204, *USA*

E. PRINCE*
Materials Science and Engineering Laboratory, National Institute of Standards and Technology, Gaithersburg, MD 20899, *USA*

AND R. TOLIMIERI†
Center for Large Scale Computation, City University of New York, New York, NY 10036-8099, *USA*

(*Received* 13 *June* 1991; *accepted* 19 *December* 1991)

Abstract

Methods are described for exploiting the symmetry of uniaxial space groups containing rotation axes of order three and higher to improve the efficiency of computation of Fourier transforms. Mapping a symmetrical two-dimensional section into four dimensions enables the selection of non-contiguous asymmetric units over which fast Fourier transforms can be performed that reduce the computation time by a factor of approximately the order of the rotation axis. The application of the procedure to plane group $p3$ and its extension to $p4$ and $p6$ are described.

Introduction

Diffraction intensities and atomic distributions in crystals are related to one another by Fourier transforms, which therefore play a major role in structural crystallography. Because of this a large fraction of the work on computational methods, throughout the history of the application of diffraction techniques to crystallography, has been directed toward improving the efficiency of computation of Fourier transforms. A major advance came with the development by Cooley & Tukey (1965; also Gentleman & Sande, 1966) of a procedure that has become known as the fast Fourier transform, or FFT. Whereas previously used methods had required numbers of operations proportional to the square of the number of Fourier coefficients, N, the number of operations required by the FFT procedure is proportional approximately to $N \log N$, which, for moderately large values of N, increases only slightly more rapidly than linearly with increasing N.

Further savings in both time and computer capacity can be achieved if a FFT routine can make use of space-group symmetry to avoid storing redundant data and

* To whom all correspondence should be addressed.

† This research was supported by the Advanced Research Projects Agency of the Department of Defense and was monitored by the Air Force Office of Scientific Research under contract no. F49620-89-0-0020. The United States Government is authorized to reproduce and distribute reprints for governmental purposes notwithstanding any copyright and notation hereon.

0108-7673/92/030346-04$03.00